Braz J Phys (2015) 45:251–257
DOI 10.1007/s13538-015-0303-5

GENERAL AND APPLIED PHYSICS

Relativistic Angular Distribution of Photoelectrons in the Tunneling Ionization of Atoms by a Linearly Polarized Laser Field

Tatjana B. Miladinović · Violeta M. Petrović

Received: 10 October 2014 / Published online: 12 February 2015

Abstract In this paper, the angular distribution of the ejected photoelectrons during relativistic tunneling ionization of atoms by linearly polarized laser field is discussed. The effect of shifted ionization potential has been taken into account. The influence of two different spatial profiles of an intense laser pulse is studied.

Keywords Relativistic angular distribution · Tunneling ionization · Polarized laser field

1 Introduction

Up to now, the theoretical description of the ionization of an atom (ion) by an external laser field concerned tunneling ionization when the intensity of the radiation field is not too strong. However, progress in laser technology in the last few years has made it possible to generate coherent electromagnetic radiation in the optical frequency range and with electric field intensity of the order up to 10^{22} W cm^{-2}. In ultra strong fields (10^{17}–10^{20} W cm^{-2}), an entire valence shell along with several inner shell electrons may be ionized [1, 2]. The laser field is so intense that it can create multivalent ions with charges Z~40–60. This opens the door to a relativistic approach.

It is known from the classical theory of the interaction of a charged particle with a plane-wave electromagnetic field that relativistic behavior will occur at sufficiently high field strength, even if the initial conditions of the particle would appear to be entirely nonrelativistic. The theory of this process was started by Keldysh [3], where the tunnel effect in an alternating electric field and the multiphoton ionization of atoms were given to be the limiting cases of photoionization process. Various modifications to Keldysh's theory have been proposed and many "Keldysh-like" models are commonly used analytical models for describing laser atom interaction. First, Perelomov et al. developed a method for calculating the probability of ionization of a bound state under the action of an alternating field, PPT theory [4, 5]. An extended version developed by Ammosov et al. (ADK theory) is derived for complex atoms and ions and for arbitrary quantum numbers of the electronic configuration [6]. Relativistic extension of the widely used ADK theory, as well as the theoretical observation of the relativistic angular spectra can be found in [7, 8]. Experimental results in this area have been given in ref. [9].

In this paper, we observed the relativistic photoelectron angular distribution's spectra with respect to the inclusion of the ponderomotive and the Stark shift in the ionized potential. The electron is always oscillating around its nucleus, but we neglected this motion in our analysis. We observed only the motion of the electron in an oscillating electric field. In case of long laser pulses, an electron is accelerated by a spatial gradient of the laser field in the direction perpendicular to the laser beam. The electron's acceleration is called ponderomotive acceleration, which changes angular and energy distribution of photoelectrons. The physical picture of this motion is mathematically described by the ponderomotive potential, which represents the time averaged kinetic energy of the electron oscillating in the laser field. The ponderomotive potential of an electron is given by the well-known expression (nonrelativistic case) $U_p^{\mathrm{nonrel}} = (1+\epsilon^2)\frac{F^2}{4\omega^2}$, where F is the field strength, ω is the angular frequency, and ϵ is ellipticity, with ϵ=0 corresponding to the linearly, and ϵ=1 to the circularly polarized laser field. The atom's energy levels are altered in the laser field. This effect is known as the Stark effect, and it

T. B. Miladinović · V. M. Petrović (✉)
Department of Physics, Faculty of Science, Kragujevac University, Radoja Domanovića 12, 34000 Kragujevac, Serbia
e-mail: violeta.petrovickg@gmail.com

must be incorporated into the ionization potential. For the case of a strong external field with small field frequency, when the following conditions are fulfilled $dF \gg \omega, \alpha F^2 \gg \omega$, where α is the static polarizability of the atom [10] and d is constant dipole moment [11], the displacement of the energy level is determined by expression $E_{\mathrm{St}} = \frac{\alpha F^2}{4}$ [12].

In addition, the laser beam spatial dependence is discussed. No matter how fast the ionization process occurs, it is dependent on the laser field strength, F. Because of that, it is convenient to consider the influence of the different beam shapes on the angular distribution of ejected photoelectrons. Therefore, we analyzed the Gaussian and the Lorentzian beam profiles.

2 Theory

Tunneling ionization is a process in which the laser field is regarded as low frequency and strong if the energy of laser photons is much lower than the ionization potential and the Keldysh adiabaticity parameter is less than unity, $\gamma_{\mathrm{nonrel}} = \sqrt{(1+\epsilon^2)E_i/2U_p^{\mathrm{nonrel}}}$, where ϵ is ellipticity, E_i is the unperturbed ionization potential, and U_p^{nonrel} is the nonrelativistic ponderomotive potential.

It is widely believed [12] that a zero frequency limit of laser-induced ionization is a tunneling limit, but it is shown that the limit $\gamma \to 0$ is extreme relativistic limit [13]. Analyses were made by taking this into account. In that case, the relativistic Keldysh parameter has the form $\gamma_{\mathrm{rel}} = \frac{\omega c}{F}\sqrt{1-\left(\left(c^2-\frac{Z^2}{2}\right)/c^2\right)^2}$, where Z is the charge state of atom, and c is the speed of light [14].

In the semiclassical model of strong-field ionization, the electron first escapes from the atom by tunneling and then in a second step, it follows a classical trajectory, influenced by the parent ion potential and laser pulse. The simplest approach is to neglect the influence of the ion potential on the electron trajectory. The expression for the rate of tunneling ionization in a linearly polarized laser field, in the nonrelativistic regime when the ejected electron has a zero initial momentum, is given by the following expression [12]:

$$W^{\mathrm{nonrel}} = \frac{F}{8\pi Z}\left(\frac{4eZ^3}{Fn^{*4}}\right)^{2n^*}\sqrt{\frac{3Fn^{*3}}{\pi Z^3}}\exp\left(\frac{2Z^3}{3Fn^{*3}}\right). \quad (1)$$

When the electron has nonzero initial momentum the aforementioned expression becomes $W_p^{\mathrm{nonrel}} = \frac{F}{8\pi Z}\left(\frac{4eZ^3}{Fn^{*4}}\right)^{2n^*}\sqrt{\frac{3Fn^{*3}}{\pi Z^3}}\exp\left(-\frac{2Z^3}{3Fn^{*3}}-\frac{p^2\gamma^3}{3\omega}\right)$ [14], where n^* is the effective quantum number, $n^*=Z/(2E_i)$, and p the initial momentum of the ejected photoelectrons.

Analysis of a strong-field laser problem should start from the relativistic formulation for the angular distribution of the ejected photoelectrons [15]:

$$W^{\mathrm{rel}} = W^{\mathrm{nonrel}}\exp(\varphi(\theta,\psi)), \quad (2)$$

where W^{nonrel} is given by Eq. (1) while θ is the angle between the direction of the ejected electron momentum and polarization axis, ψ is the azimuthal angle and the function $\varphi(\theta,\psi)$ is defined as [15]:

$$\varphi(\theta,\psi)\frac{4}{3}\frac{\sqrt{E_i^3E_e}}{Fc}\left(\frac{3E_e}{E_i}-1\right)\theta\sin\psi, \quad (3)$$

where E_e is the kinetic energy of the ejected photoelectrons: $E_e = \sqrt{p^2c^2+c^4}-c^2$. As the intensity is raised, the barrier becomes thinner and lower and the bound electron can tunnel through the barrier. Just after leaving the barrier, the momentum of the ejected photoelectron is p. The ionization probabilities in static and alternating electric field are different only by the pre-exponential factor [4]. Because of that, it is convenient to use the parabolic coordinate to express initial momentum outside of barrier, $p = \frac{1}{2}\left(\sqrt{F\eta-1}-\frac{1}{\eta\sqrt{F\eta-1}}\right)$, where η is the parabolic coordinate, $\eta > 1/F$ [16]. If a system's total energy is independent of the coordinate η, then momentum is conserved along the classical path [17].

From Eq. (3), we can determine two energy ranges: low energies $3E_e<E_i$ and high energies $3E_e>E_i$. The angular distribution is asymmetric in each range. If we assume that the value of the electron kinetic energy is much larger than the ionization potential, therefore, we have $3E_e>E_i$ and then the transition rate dependence on the electron ejection angles has the following form [15]:

$$W^{\mathrm{rel}} = W^{\mathrm{nonrel}}\exp\left[\left(-\frac{2E_e\sqrt{2E_i}}{F}\right)\theta^2+\left(4\frac{\sqrt{E_e^3E_i}}{Fc}\right)\theta\sin\psi\right]. \quad (4)$$

In the range of azimuthal angles $0<\psi<\pi$, the index of the exponent has a maximum. In this range the maximal electron's ejection angle, θ, is defined as $\theta_m = \sqrt{E_e/2c^2}\sin\psi \ll 1$. Taking this into account, Eq. (4) can be rewritten as $W^{\mathrm{rel}} = W^{\mathrm{nonrel}}\exp\left[\left(\sqrt{2E_i}E_e^2/\sqrt{2}Fc^2\right)\sin^2\psi\right]\exp\left[\left(-2E_e\sqrt{2E_i}/F\right){\theta_m}^2\right]$, i.e., in the form:

$$W^{\mathrm{rel}} = W_{\max}(\psi)\exp\left(-\frac{2E_e\sqrt{2E_i}}{F}\right){\theta_m}^2, \quad (5)$$

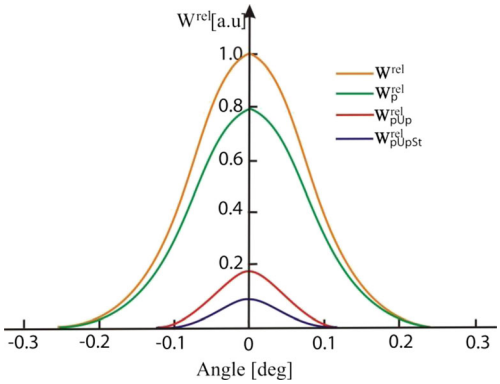

Fig. 1 The theoretical curves for the relativistic angular distribution spectra, W^{rel}, versus the scattering angle, θ_m for $W^{\mathrm{rel}}, W_p^{\mathrm{rel}}$, $W_{p\mathrm{Up}}^{\mathrm{rel}}$ and $W_{p\mathrm{UpSt}}^{\mathrm{rel}}$. The value of η is fixed at 0.2 and the laser field intensity is $I{=}10^{18}$ W cm^{-2}

where $W_{\max}(\psi)$ is the maximum value of the transition rate that occurs at the angle of θ_m, $W_{\max}(\psi) = W^{\mathrm{nonrel}}\exp\left[\left(E_e^2\sqrt{2E_i}/\sqrt{2}Fc^2\right)\sin^2\psi\right]$.

Equations (4) and (5) suggest that W^{rel} depends on the ionization potential, E_i. However, a laser irradiation changes the ionization potential of an atom. When the laser field intensity increases the change of the ionization potential becomes more significant. Here we considered two effects: the ponderomotive potential and the Stark effect in the relativistic domain.

The relativistic ponderomotive potential may be written in the following form [18] $U_p^{\mathrm{rel}} = \sqrt{c^4 + 2c^2U_p^{\mathrm{nonrel}}} - c^2$, where U_p^{nonrel} is a nonrelativistic ponderomotive potential. The Stark effect has the same form, E_{St}, as in the nonrelativistic domain. To account for these two effects, we replaced the unperturbed relativistic ionization potential $E_i = c^2 - \sqrt{c^4 - Z^2c^2}$ [19] with the shifted, corrected relativistic effective ionization potential:

$$E_{\mathrm{ief}}^{\mathrm{rel}} = c^2 - \sqrt{c^4 - Z^2c^2} + \left(\sqrt{c^4 + 2c^2U_p^{\mathrm{nonrel}}} - c^2\right) + \alpha F^2/4. \tag{6}$$

Next, we inserted Eq. (6) into Eq. (5) and rewrote the relativistic angular distribution in the following form:

$$W^{\mathrm{rel}} = W_{\max}(\psi)\left(-\frac{2\left(\sqrt{p^2c^2 + c^4} - c^2\right)\sqrt{2\left(c^2 - \sqrt{c^4 - Z^2c^2} + \left(\sqrt{c^4 + 2c^2U_p^{\mathrm{nonrel}}} - c^2\right) + \alpha F^2/4\right)}}{F}\right)\theta_m{}^2. \tag{7}$$

Finally, we introduced the width of the relativistic photoelectron energy distribution as $\Delta E = c\sqrt{\omega/\gamma}$ [20].

3 Effect of Laser Spatial Profile

The quality of a laser beam is a topic of interest to both designers and users of optical systems. Different aspects of the beam quality may have higher priority in various optical systems. Suitable mathematical models for the different beam shapes are either Gaussian or Lorentzian functions, the choice between the two functions being dictated by the statistical properties of the light-generating process. In the general case, the electric field strength of an electromagnetic wave is a function of spatial coordinates and time. Often, such functional dependence can be factorized and the electric field can be represented as a product of two functions depending on spatial coordinates and time, respectively. Here, we are interested in the influence of the spatial profile in the variables considered.

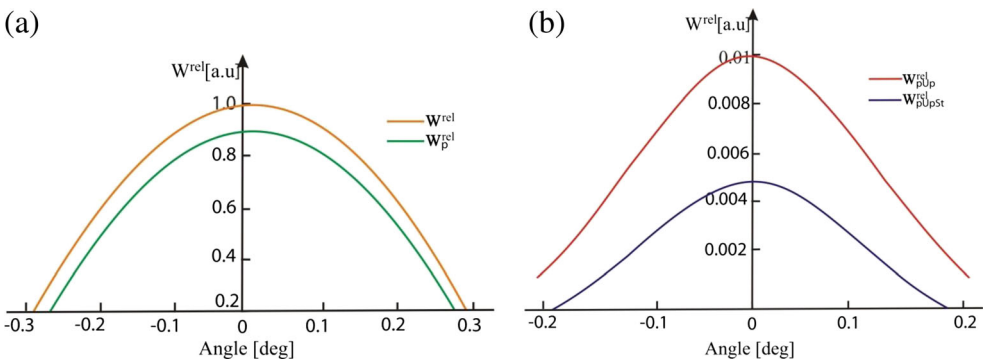

Fig. 2 The theoretical curves for the relativistic angular distribution spectra, W^{rel} versus the scattering angle, θ_m. **a** W^{rel} and W_p^{rel} W^{rel}, **b** $W_{p\mathrm{Up}}^{\mathrm{rel}}$ and $W_{p\mathrm{UpSt}}^{\mathrm{rel}}$. The value of the parabolic coordinate η is fixed at 0.2

Common standard for an ideal laser is one with a single Gaussian spatial mode [21]:

$$F(\rho) = F\exp\left(-\left(\frac{\rho}{R}\right)^2\right), \tag{8}$$

where ρ is the axial coordinate that is normal to the light ray, $\rho = R\sqrt{1+\left(\frac{\lambda\eta}{\pi R^2}\right)}$ [22] and R is the radius of laser beam.

Taking Eq. (8) into account, the relativistic angular distribution of ejected photoelectrons can be written as:

$$W^{\mathrm{relG}} = W_{\max}(\psi)\left(-\frac{2\left(\sqrt{p^2c^2+c^4}-c^2\right)\sqrt{2\left(c^2-\sqrt{c^4-Z^2c^2}+\left(\sqrt{c^4+2c^2(1+\epsilon^2)\left(F\exp\left(-(\rho/R)^2\right)\right)^2/4\omega^2}-c^2\right)+\alpha\left(F\exp\left(-(\rho/R)^2\right)\right)^2/4\right)}}{F\exp\left(-(\rho/R)^2\right)}\right)\theta_m{}^2 . \tag{9}$$

We also considered the Lorentzian spatial profile. From several profiles which can be found, in this paper, we used the following [23]:

$$F(\rho) = \frac{F}{\left(1+\left(\frac{\rho}{R}\right)^2\right)}. \tag{10}$$

With this spatial assumption, the relativistic angular distribution becomes:

$$W^{\mathrm{relL}} = W_{\max}(\psi)\left(-\frac{2\left(\sqrt{p^2c^2+c^4}-c^2\right)\sqrt{2\left(c^2-\sqrt{c^4-Z^2c^2}+\left(\sqrt{c^4+2c^2(1+\varepsilon^2)\left(F/\left(1+(\rho/R)^2\right)\right)^2/4\omega^2}-c^2\right)+\alpha F^2/4\left(1+(\rho/R)^2\right)^2\right)}}{F/\left(1+((\rho/R))^2\right)}\right)\theta_m{}^2 . \tag{11}$$

4 Analysis

We performed the analysis of the relativistic angular distribution of ejected photoelectrons with respect to the corrections of the ionization potential for different angles at fixed field intensities. The laser field intensity varied between $I=10^{18}$ and $I=10^{20}$ W cm^{-2}. These intensities correspond to the field strengths F in interval 10^9–10^{10} V cm^{-1}. We considered the case of atom argon, *Ar*, for ionized second shell, $Z=10$. The atomic system of units is used $e = m_e = \hbar = 1$, $c=137$ [a.u.]. In the regime of very low Keldysh parameter $\gamma \ll 1$ and the wavelength of the incident light $\lambda=800$ nm ($\omega=0.05696$ a.u) ionization in a strong field can be successfully described as tunneling process. Therefore, we performed our discussion for $\gamma=0.08$. Short pulses are assumed. The relativistic contributions to observed variables are included through the relativistic expressions for appropriate variables and through the effective ionization potential. All theoretical curves correspond to the azimuthal angle of $\psi=\pi/2$.

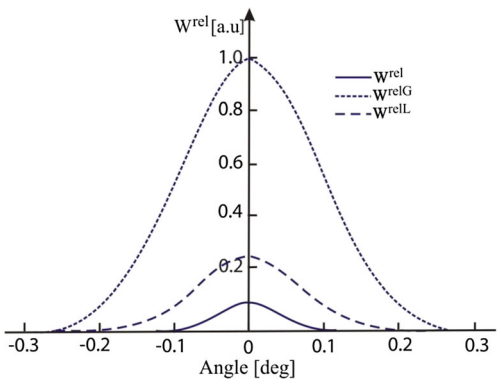

Fig. 3 The relativistic angular distributions of ejected electrons, W^{rel}, as a function of the scattering angle, θ_m, for the general, Gaussian and Lorentzian laser beam shapes for the fixed value of the laser field $I=10^{18}$ W cm^{-2} and the parabolic coordinate $\eta=0.2$

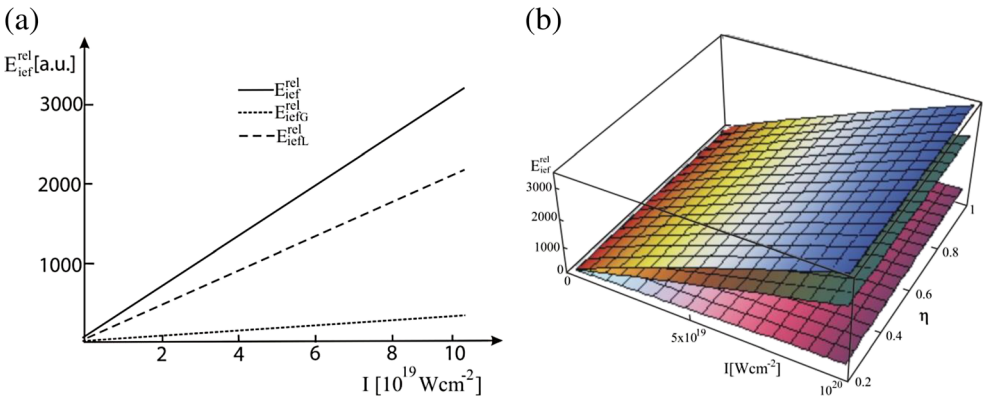

Fig. 4 The relativistic effective ionization potential $\boldsymbol{E}^{\mathrm{rel}}_{\mathrm{ief}}$ for different laser profiles, $\boldsymbol{E}^{\mathrm{rel}}_{\mathrm{ief}\boldsymbol{G}}$ and $\boldsymbol{E}^{\mathrm{rel}}_{\mathrm{ief}\boldsymbol{L}}$: **a** 2D graph, for fixed η=1 and $10^{18} < I < 10^{20}$W cm^{-2}, **b** 3D graph, for 0.2<$\boldsymbol{\eta}$<1 and 10^{18} <I<10^{20} W cm^{-2}

Figure 1 demonstrates the dependence of the relativistic angular distribution, W^{rel} (see Eq. 7), on the scattering angle for the fixed laser field intensity I=10^{18} W cm^{-2}. Here and in the following we used the notation: superscript is the same for all variables and marks the relativistic angular distribution, W^{rel}. Variable without subscript is value of W^{rel} without any correction, subscript "p" notes the transition rate with included initial momentum, W^{rel}_{p} (see Eq. 5 for $W_{\max}(\psi)$ and W^{nonrel}_{p}), $W^{\mathrm{rel}}_{p\mathrm{Up}}$ marks the transition rate with included ponderomotive potential and $W^{\mathrm{rel}}_{p\mathrm{UpSt}}$ with the ponderomotive potential and the Stark shift (see Eq. 6).

This dependence shows that the probability to find an electron in the region with the scattering angle bigger than approximately 0.25 ° for W^{rel}_{p} and W^{rel}_{p} i.e., 0.1° for W^{rel}_{pUp} and $W^{\mathrm{rel}}_{p\mathrm{UpSt}}$ approaches zero. Within the entire angle range, decreasing of the relativistic angular distribution is exponential. In addition, it can be seen that the maximal value of the angular probability decreases. The physical reason for this is the ponderomotive and the Stark shift affecting the unperturbed ionization potential.

In Fig. 2, we investigated how increasing the laser field intensity influences the behavior of curves of the relativistic angular distribution, W^{rel}. Now, the field intensity was I= 10^{19} W cm^{-2}.

We separated curves in two graphs because the mentioned corrections caused significant decrease of the relativistic angular distribution at the higher field intensity for the same scattering angles. The range at which ejected photoelectrons could be found is reduced. The behavior of curves shows some deviation from generally expected "Gaussian" flow for the cases W^{rel} and W^{rel}_{p}.

To complete the picture of the observed effects, we compared the relativistic angular distribution with the assumption of a different spatial laser pulse shape. Figure 3 shows the calculated relativistic angular distribution's probabilities, W^{rel} (see Eq. 7) for general case, i.e., for generally assumed laser beam shape, without any specifications and for specified beam shapes: Gaussian and Lorentzian (see Eqs. 9 and 11). Index "G" (respectively, "L") indicates assumption of the Gaussian (respectively, the Lorentzian) beam shape.

We plotted curves for the case when all corrections are taken into account, meaning that the theoretical angular distribution curves of ejected photoelectrons in Fig. 3 are obtained on the assumption that all electrons were accelerated by the ponderomotive potential with a nonzero initial momentum and included Stark shift. As can be seen from Fig. 3 in the range of the scattering angle (−0.3<θ<0.3) the assumption of a Gaussian form laser pulse gives the biggest value of observed relativistic angular probability. This range is wider than those for Lorentzian and general beam profile. For all three cases, the shape of curves is very similar.

Within the above specified range of the laser field intensities we applied these profiles to the relativistic effective

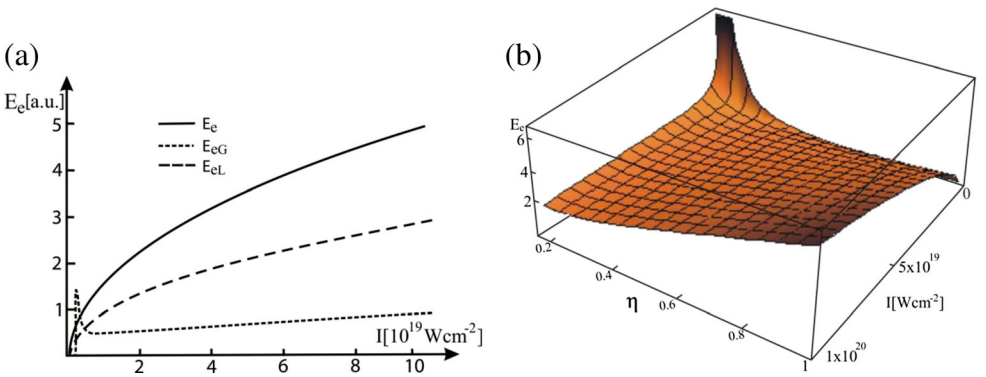

Fig. 5 The kinetic energy of the ejected photoelectron: **a** 2D graph, E_e, E_{eG} and E_{eL} versus the laser field intensity at the fixed value of parabolic coordinate η= 1, **b** 3D graph E_{eG} for 0.2<$\boldsymbol{\eta}$<1 and 10^{18}<I<10^{20}Wcm^{-2}

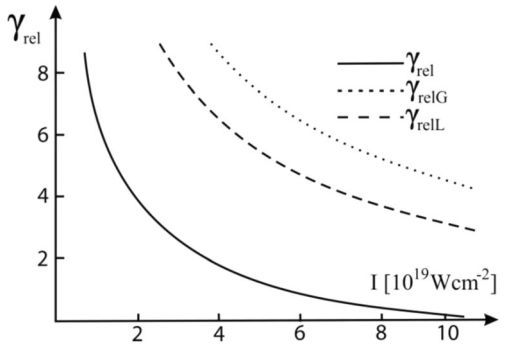

Fig. 6 Keldysh parameter, γ_{rel} versus the laser field intensity the Gaussian, γ_{relG} and the Lorentzian, γ_{relL}, laser beam profile

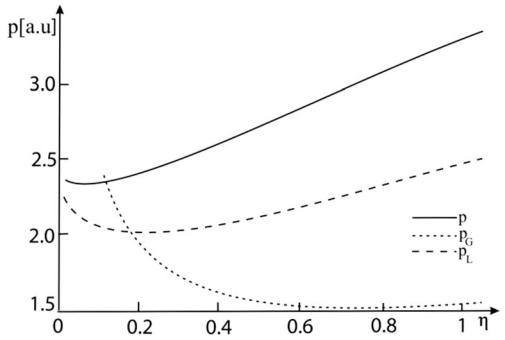

Fig. 8 Initial momentum of the ejected electron versus the parabolic coordinate η at fixed field intensity $I=10^{20}$ W cm^{-2} for different laser beam shapes

potential (see Eq. 6) and obtained the following expressions, for the Gaussian beam:

$$E_{ie\,fG}^{rel} = c^2 - \sqrt{c^4 - Z^2c^2} + \left(\sqrt{c^4 + \frac{2c^2\left(F\exp\left(-(\rho/R)^2\right)\right)^2}{4\omega}} - c^2 \right) + \alpha\left(F\exp\left(-(\rho/R)^2\right)\right)^2/4, \quad (12)$$

and for the Lorentzian:

$$E_{ie\,fL}^{rel} = c^2 - \sqrt{c^4 - Z^2c^2} + \left(\sqrt{c^4 + 2c^2\frac{\left(\boldsymbol{F}/\left(1+(\boldsymbol{\rho}/\boldsymbol{R})^2\right)\right)^2}{4\omega}} - c^2 \right) + \alpha\left(\boldsymbol{F}/\left(1+(\boldsymbol{\rho}/\boldsymbol{R})^2\right)\right)^2/4. \quad (13)$$

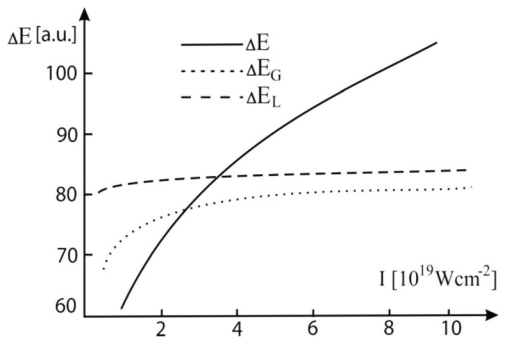

Fig. 7 The relativistic energy spectrum's width, ΔE, versus the laser field intensity given for the general, the Gaussian and the Lorentzian laser beam profile

In Fig. 4, we show the relativistic effective ionization potential calculated based on Eqs. (6), (12), and (13), respectively:

Also, we analyzed how aforementioned corrections in combination with the specified spatial profile influence the kinetic energy of the ejected photoelectrons, energy width, as well as the initial momentum.

Figure 5a, 2D graph, presents the theoretical curves for the kinetic energy of the ejected photoelectrons, E_e, for the different laser beam profiles, E_{eG} and E_{eL}, obtained by including Eqs. (8) and (10) in the expression for E_e as a function of the laser field intensity. Figure 5b, 3D graph, presents the dependence of E_{eG} on the laser field intensity and the parabolic coordinate η.

For the Gaussian beam, the kinetic energy reaches maximal value while for the other two cases, the theoretical curves are monotonically increasing functions with very similar slope.

Figure 6 demonstrates relativistic Keldysh parameter γ_{rel}. Continuous curves are obtained based on expression for γ_{rel} in combination with Eqs. (8) and (10):

We observed similarity in behavior of lines. With increasing field amplitude γ_{rel} comes along very close to the zero value in accordance with Reiss [24].

In Fig. 7, the dependence of the relativistic energy spectrum's width, ΔE, of the field intensity, for different laser beam shape (see Eqs. (8) and (10)), is shown:

It can be seen that the relativistic energy spectrum's width is sensitive to the laser beam shape. Specified profile caused narrower spectrum width.

Finally, Fig. 8 gives the results of a calculation carried out based on the equation for the initial momentum of the ejected electron and involving the spatial distribution of the radiation intensity (see Eqs. (8) and (10)).

Obtained results for the initial momentum of the ejected photoelectrons are in accordance with results presented in Fig. 3. Higher initial momentum causes lower probability of the relativistic angular distribution.

5 Conclusion

In this paper, the relativistic semiclassical ionization of an atom in the presence of intense linearly polarized laser light has been considered. The theoretical approach employed in the paper predicts that the electron angular distribution spectra are changed by including the specified effects such as the initial momentum, ponderomotive and Stark shift. We can state that incorporation of these effects leads to significant decreasing of the relativistic angular distribution of ejected electrons on the given angle. Also, a theoretical analysis showed a sensitivity of all observed variables to the laser beam shape.

Acknowledgments We are grateful to the Serbian Ministry of Education, Science and Technological Development for financial support through Projects 171020 and 171021.

References

1. E.A. Chowdhury, C.P.J. Barty, B.C. Walker, Phys Rev A **63**, 042712 (2001)
2. K. Yamakawa et al., Phys Rev Lett **92**, 123001 (2004)
3. L.V. Keldysh, Z. Eksp, Teor Fiz **47**, 1945 (1964)
4. A.M. Perelomov, V.S. Popov, M.V. Terentíev, Sov Phys JETP Lett **23**, 924 (1966)
5. A.M. Perelomov, V.S. Popov, M.V. Terentíev, Sov Phys JETP Lett **24**, 207 (1967)
6. M.V. Ammosov, N.B. Delone, V.P. Krainov, Sov Phys JETP Lett **64**, 1191 (1986)
7. V.P. Krainov, B. Shokri, Laser Phys **5**(4), 793 (1995)
8. V.P. Krainov, A.V. Sofronov, Laser Phys **14**(3), 401 (2004)
9. A.D. Di Chiara, I. Ghebregziabher, R. Sauer, J. Waesche, S. Palaniyappan, B.L. Wen, B.C. Walker, Phys Rev Lett **101**, 173002 (2008)
10. http://ctcp.massey.ac.nz/Tablepol2014.pdf
11. N.B. Delone, V.P. Krainov, *Multiphoton processes in atoms*, 2nd edn. (Springer, New York, 2000), p. 14
12. M.V. Ammosov, N.B. Delone, V.P. Krainov, Zh Eksp Teor Fiz **91**, 2008 (1986)
13. D.F. Ye et al., J Phys B Atomic Mol Opt Phys **43**, 235601 (2010)
14. V.M. Ristić, T.B. Miladinović, M.M. Radulović, Laser Phys **18**, 1183 (2008)
15. N.B. Delone, I.Y. Kiyan, V.P. Krainov, Laser Phys **3**(2), 312 (1993)
16. D. Bauer, *Theory of intense laser-matter interaction* (Max-Planck Institute, Heidelberg, 2006), p. 58
17. L. D. Landau and E. M. Lifshitz, *Quantum mechanics: non-relativistic theory*, 3rd ed. (Pergamon, Oxford, 1991), § 77, p. 298
18. I. Ghebregziabher, Radiation and photoelectron dynamics in ultrastrong laser fields, Pro Quest, 36 (2008)
19. E. Yakaboylu, M. Klaiber, H. Bauke, K.Z. Hatsagortsyan, H.K. Christoph, Phys Rev A **88**, 063421 (2013)
20. N.B. Delone, V.P. Krainov, Physics-Uspekhi **41**(5), 469 (1998)
21. I.I. Bondar, V.V. Suran, D.I. Bondar, Phys Rev A **88**, 023407 (2013)
22. http://www.colorado.edu/physics/phys3340/phys3340_sp12/CourseInformation/Optics/Gaussian%20Beams%20Lab%20Guide.pdf
23. S. L. David and H. A. John, 2005, SPIE Conf. Laser Beam Shaping VI, Proc. 5876; http://www.diss.fuberlin.de/diss/servlets/MCRFileNodeServlet/FUDISS_derivate_000000005776/09_Chapter05.pdf
24. H.R. Reiss, Phys Rev A **82**, 023418 (2010)